IX Fluidization by lift: single particle studies[1]

In Sections VI, VII and VIII we discussed fluidization and sedimentation in which the flow is parallel to gravity and is governed by a balance of buoyant weight and drag. Now we turn to flows perpendicular to gravity in which the particles are levitated against their buoyant weight by lift forces perpendicular to the flow.

The theory of lift is one of the great achievements of aerodynamics. Airplanes take off, rise to a certain height, and move forward under a balance of lift and weight. The lift and suspension of particles in the flow of slurries is another application in which lift plays a central role; in the oil industry we can consider the removal of drill cuttings in horizontal drill holes and sand transport in fractured reservoirs. The theory of lift for these particle applications is undernourished and in most simulators no lift forces are modeled.

Problems of fluidization by lift can be decomposed into two separate types of study: (1) single particle studies in which the factors that govern lifting of a heavier-than-liquid particle off a wall by a shear flow are identified and (2) many particle studies in which cooperative effects on lift-off and hindered settling are important.

Our study of single particle lift starts by looking at a particle on the bottom wall of a plane channel. The fluid in the channel is driven by a pressure gradient. We want a qualitative description of the levitation of the particle as the pressure gradient is increased. The description will be carried out in two dimensions here and then compared with computed results from DNS.

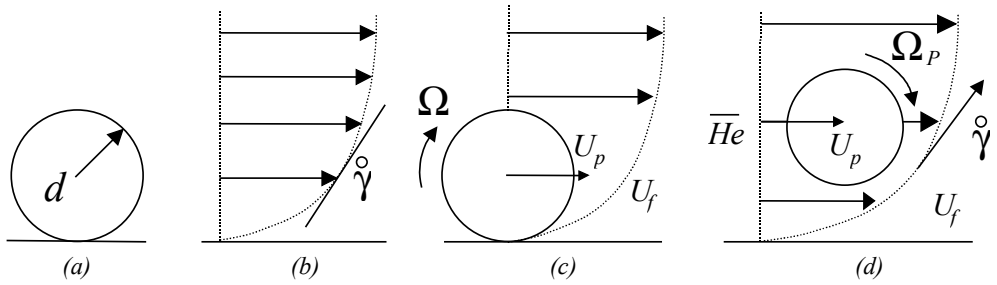

Figure IX.1 Lift off and levitation to equilibrium.

i. The pressure on a particle is increased

ii. The particle slides and rolls

iii. At a critical speed the particle lifts off

iv. It rises to a height in which the lift balances the weight

v. It moves forward under zero net force and torque; the particle does not accelerate (see IX.9)

After the particle lifts off, it rises to a height h_e in which lift balances weight. Then the slip velocity $\mathbf{U}_f - \mathbf{U}_p$ and angular slip velocity $\Omega_f - \Omega_p = \dot{\gamma}/2 - \Omega_p$ are positive and at equilibrium

[1] This chapter is based in part on results reported in the paper by Patankar, Huang, Ko and Joseph 2001.

values as shown in figure IX.1(d). In many of the calculated cases the equilibrium is steady, but for faster flows we have found periodic motions associated with Hopf bifurcation; surely there are more complicated dynamics for turbulent regimes.

▪ Equations of motion and dimensionless parameters

The problem to be considered is the levitation of a circular particle in a plane Poiseuille flow in a horizontal channel. A particle of diameter d rests on the bottom wall at $y = 0$ of a horizontal channel of width W (see figure IX.2). A flow is induced by a pressure gradient. The pressure drop must balance the force due to the wall shear stress; $\dot{\gamma} = du/dy$ is the shear rate, $\dot{\gamma}_w$ is the shear rate at the wall $y = 0$, all when there are no particles in the flow. We use

$$R = \frac{\mathring{\gamma}_w d^2}{\nu}, \nu = \frac{\eta}{\rho_f} \tag{IX.1}$$

to index different flows. The equations of motion (II.6, 7, 8) are modified to include the effects of an applied pressure gradient P given by (III.2).

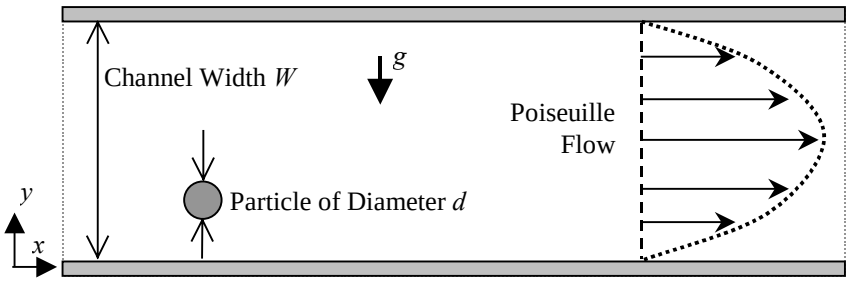

Figure IX.2. The particle is heavier than the fluid and lifts off the bottom y *= 0 as the pressure gradient, indexed by* $\dot{\gamma}_w$*, is raised past a critical value, lift-off value.*

There are features of the problem of levitation of circular particles in a horizontal plane Poiseuille flow which require explanation. The equations of motion for fluid and particle are given in general terms by (II.1) through (II.5). In the present case it is necessary to explain how the pressure is decomposed for computation on a periodic domain. It is understood that the velocity **u** is solenoidal, div **u** = 0 and we have changed p to P where P is the mean normal stress. We have

$$\rho_f \left[\frac{\partial \mathbf{u}}{\partial t} + (\mathbf{u} \cdot \nabla)\mathbf{u} \right] = -\nabla P + \eta \nabla^2 \mathbf{u} + \rho_f \mathbf{g} \tag{IX.2}$$

where **u** satisfies no-slip conditions at solid boundaries. The equations of motion of the solid particles are given by

$$\rho_p V_p \frac{d\mathbf{U}}{dt} = \rho_p V_p \mathbf{g} + \oint \{-P\mathbf{1} + 2\eta \mathbf{D}[\mathbf{u}]\} \cdot \mathbf{n}\, d\Gamma$$
$$\mathrm{I}\frac{d\boldsymbol{\Omega}}{dt} = \oint (\mathbf{x} - \mathbf{X}) \wedge [(-P\mathbf{1} + 2\eta \mathbf{D}[\mathbf{u}]) \cdot \mathbf{n}\,]\, d\Gamma \qquad \text{(IX.3)}$$

where **u** is the velocity of the mass center and $\boldsymbol{\Omega}$ is the angular velocity.

The Poiseuille flow problem studied in the computation is an idealization of a channel flow problem in which pressure is prescribed at the inlet x_1 and outlet x_2, $x_2 >> x_1$ where $P_1 > P_2$. The prescribed inlet-outlet conditions are modeled by a prescribed pressure gradient

$$\overline{p} = \frac{P_1 - P_2}{x_2 - x_1}. \qquad \text{(IX.4)}$$

We decompose the pressure into a periodic part $p(x, y, t)$, hydrostatic part $\rho_f \mathbf{g} \cdot \mathbf{x}$ and the constant pressure gradient part $-\overline{p}\mathbf{e}_x \cdot \mathbf{x} = -\overline{p}x$, thus

$$P = p + \rho_f \mathbf{g} \cdot \mathbf{x} - \overline{p}\mathbf{e}_x \cdot \mathbf{x}\ . \qquad \text{(IX.5)}$$

Combining (IX.5) with (IX.2) and (IX.3) we get

$$\rho_f \left[\frac{\partial \mathbf{u}}{\partial t} + (\mathbf{u} \cdot \nabla)\mathbf{u} \right] = -\nabla p + \eta \nabla^2 \mathbf{u} + \overline{p}\mathbf{e}_x \qquad \text{(IX.6)}$$

$$\rho_p V_p \frac{d\mathbf{U}}{dt} = (\rho_p - \rho_f) V_p \mathbf{g} + V_p \overline{p}\mathbf{e}_x + \oint \{-p\mathbf{1} + 2\eta \mathbf{D}[\mathbf{u}]\} \cdot \mathbf{n}\, d\Gamma \qquad \text{(IX.7)}$$

$$\mathrm{I}\frac{d\boldsymbol{\Omega}}{dt} = \oint (\mathbf{x} - \mathbf{X}) \wedge [(-p\mathbf{1} + 2\eta \mathbf{D}[\mathbf{u}]) \cdot \mathbf{n}]\, d\Gamma \qquad \text{(IX.8)}$$

where $V_p = \pi a^2$ is the volume per unit length of the circles and $\mathrm{I} = \rho_p \pi a^4 / 2$.

The functions $\mathbf{u}(x, y, t)$, $p(x, y, t)$, $\mathbf{U}(X, Y, t)$ and $\boldsymbol{\Omega}(X, Y, t)$ are periodic function of **x** and **X** with period *L***.** For steady flow $d\boldsymbol{\Omega}/dt = 0$ and $d\mathbf{U}/dt = 0$ for which

$$(\rho_p - \rho_f) V_p \mathbf{g} + V_p \overline{p}\mathbf{e}_x + \oint \{-p\mathbf{1} + 2\eta \mathbf{D}[\mathbf{u}]\} \cdot \mathbf{n}\, d\Gamma = \mathbf{O}. \qquad \text{(IX.9)}$$

The vertical component of (IX.9) represents the balance of lift and buoyant weight. The $\mathbf{e}_x$ component of (IX.9) balance the forward pressure gradient thrust against the $\mathbf{e}_x$ resultant of the periodic stress.

The diameter *d* is introduced as the scale of length, *V* is the scale of the velocity, *d/V* is the scale for time, $\eta V/d$ is the scale of stress and pressure and *V/d* is the scale for angular velocity. After introducing these scales into (IX.6~8), we find that

$$\left.\begin{aligned} R[\frac{\partial \mathbf{u}}{\partial t}+(\mathbf{u}\cdot\nabla)\mathbf{u}] &= -\nabla p+\frac{2d}{W}\mathbf{e}_x+\nabla^2\mathbf{u} \\ \frac{\rho_p}{\rho_f}R\frac{V_p}{d^3}\frac{d\mathbf{U}}{dt} &= -G\frac{V_p}{d^3}\mathbf{e}_y+\frac{Ld}{W}\frac{V_p}{d^3}\mathbf{e}_x+\oint\{-p\mathbf{1}+2\eta\mathbf{D}[\mathbf{u}]\}\cdot\mathbf{n}\,d\Gamma \\ \frac{\rho_p}{\rho_f}\frac{\mathbf{I}R}{\rho_p d^5}\frac{d\boldsymbol{\Omega}}{dt} &= \oint(\mathbf{x}-\mathbf{X})\wedge(-p\mathbf{1}+2\eta\mathbf{D}[\mathbf{u}])\cdot\mathbf{n}\,d\Gamma. \end{aligned}\right\} \qquad \text{(IX.10)}$$

Equation (IX.10) holds in two dimensions. The particle equations of motion can be formed for cylinders of length d; then $V_p = d\bullet\pi d^2/4$ and $I_p = d\bullet\rho_p\pi d^4/32$ and

$$\frac{\rho_p}{\rho_f}R\frac{d\mathbf{U}}{dt} = -G\mathbf{e}_y+2\frac{d}{W}\mathbf{e}_x+\frac{4}{\pi}\int_0^{2\pi}\{-p\mathbf{1}+2\eta\mathbf{D}[\mathbf{u}]\}\cdot\mathbf{n}\frac{d\theta}{2} \qquad \text{(IX.11)}$$

$$\frac{\rho_p}{\rho_f}R\frac{d\boldsymbol{\Omega}}{dt} = \frac{32}{\pi}\int_0^{2\pi}(\mathbf{x}-\mathbf{X})\wedge\{-p\mathbf{1}+2\eta\mathbf{D}[\mathbf{u}]\}\cdot\mathbf{n}\frac{d\theta}{2}\ . \qquad \text{(IX.12)}$$

The flow is determined by four dimensionless groups

$$\frac{\rho_p}{\rho_f},\ \frac{2d}{W},\ R=\frac{\rho_f\overset{\circ}{\gamma}_w d^2}{\eta},\ G=\frac{d(\rho_p-\rho_f)g}{\overset{\circ}{\gamma}_w\eta}\ . \qquad \text{(IX.13)}$$

For fixed ρ_p/ρ_f and d/W, all flows with the same R and G are dynamically similar. The density ratio ρ_p/ρ_f appears as an independent parameter only as a coefficient of particle acceleration in equations (IX.11) and (IX.12). This parameter does not enter into steady motion. Heavy particles accelerate more slowly than light ones.

The gravity Reynolds number

$$R_G = RG = \frac{\rho_f(\rho_p-\rho_f)gd^3}{\eta^2} \qquad \text{(IX.14)}$$

is independent of $\dot{\gamma}_w$; it is based on the sedimentation velocity $U_{sed} = (\rho_p - \rho_f)gd^2/18\eta$ of a sphere in Stokes flow and measures the ratio of buoyant weight to viscous effects. The particle will fall rapidly when R_G is large. The ratio

$$\frac{R}{G} = \frac{d\overset{\circ}{\gamma}_w^{\,2}}{\left(\frac{\rho_p}{\rho_f}-1\right)g} \qquad \text{(IX.15)}$$

is independent of η; this ratio, which measures the ratio of lift to buoyant weight, is a generalized Froude number; particles will rise more when R/G is large.

All the calculations have been carried in dimensional variables using CGS units. The height of the channel W is 12d (unless otherwise specified) and d = 1 cm. The length of the periodic channel L is 22d for single particle simulations and 63d for simulations of the fluidization of 300 particles. Computed quantities become independent of L for large L, and 22d and 63d are large enough. The results of calculations in dimensional variables may be generalized by post-processing in the dimensionless parameters defined above.

The undisturbed Poiseuille flow is given by

$$U(y) = 4U_m \frac{y}{W}\left(1-\frac{y}{W}\right), \qquad \dot{\gamma} = \frac{du}{dy},$$
$$U_m = U\left(\frac{W}{2}\right) = \frac{W^2 \overline{p}}{8\eta}, \qquad \dot{\gamma}_w = \frac{4U_m}{W} = \frac{W\overline{p}}{2\eta}. \tag{IX.16}$$

The calculation was carried in two channels: W/d = 12 and W/d = 48. The period of the periodic solution in the channel W/d = 12 is L/d = 22; for W/d = 48, L/d = 88.

▪ Lift-off of a single particle in plane Poiseuille flows of a Newtonian fluid

In figure IX.3 we plot the trajectory of the circular particle as a function of the distance traveled along the axial direction. The channel dimensions are: W/d = 12 and L/d = 22, where d = 1 cm (figure IX.2). The fluid density and viscosity are 1 g/cc and 1 poise, respectively. The particle density is 1.01 g/cc and R_G = 9.81. The center of the particle is initially at y = 0.6d. When R < 2.83 the particle falls to the bottom wall. For R > 2.83 it falls or rises to an equilibrium height h_e at which the buoyant weight balances the hydrodynamic lift. Thus the critical value of R for lift-off in this case is 2.83. The equilibrium height increases with R (figure IX.3).

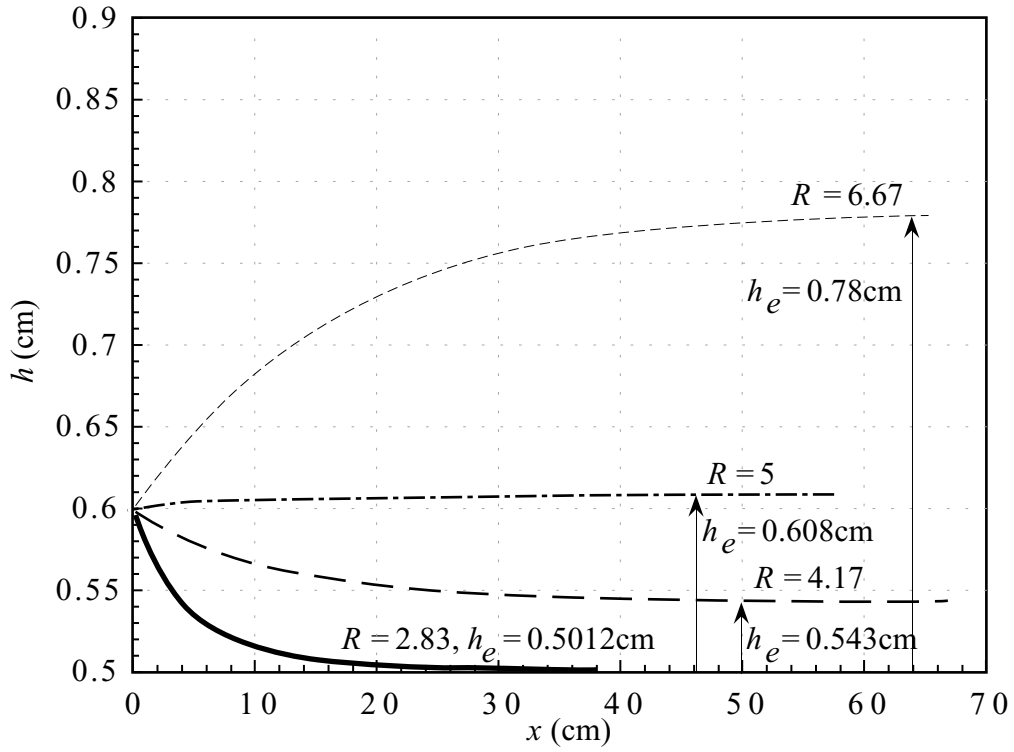

Figure IX.3. Cross stream migration of a single particle ($\rho_p > \rho_f$). A single particle of diameter d = *1 cm is released at a height of 0.6*d *in a Poiseuille flow. It migrates to an equilibrium height* h_e.

When the motion of the particle is steady, the acceleration terms in equations (IX.11, 12) vanish, and the density ratio ρ_p/ρ_f can be eliminated from the list (IX.13) of controlling parameters. We compute the critical shear Reynolds number for lift off from a steady flow. In the simulations, the smallest allowable gap size is set at 0.005*d*. The gap between the particle and the wall can never be zero (Hu and N. Patankar 2001). The smallest shear Reynolds number at which we observe an equilibrium height greater than 0.5005*d* is therefore identified as the critical shear Reynolds number for lift-off in our dynamic simulations. In most cases the smallest equilibrium height we obtain is around 0.501*d*.

The non-dimensional equilibrium height, h_e/d, is a function of R, R_G and W/d. Figure IX.4a shows the plot of h_e/d as a function of R at different values of R_G with W/d = 12. The equilibrium height increases as the shear Reynolds number is increased at all values of R_G. A larger shear Reynolds number is required to lift a heavier particle to a given equilibrium height. Figure IX.4b compares the equilibrium height of a particle of given density in channels of different widths (W/d = 12, 24 and 48). L/d = 44 for a channel with W/d = 24 whereas L/d = 88 for W/d = 48. At a given shear Reynolds number the dimensionless equilibrium height is larger for the bigger channel.

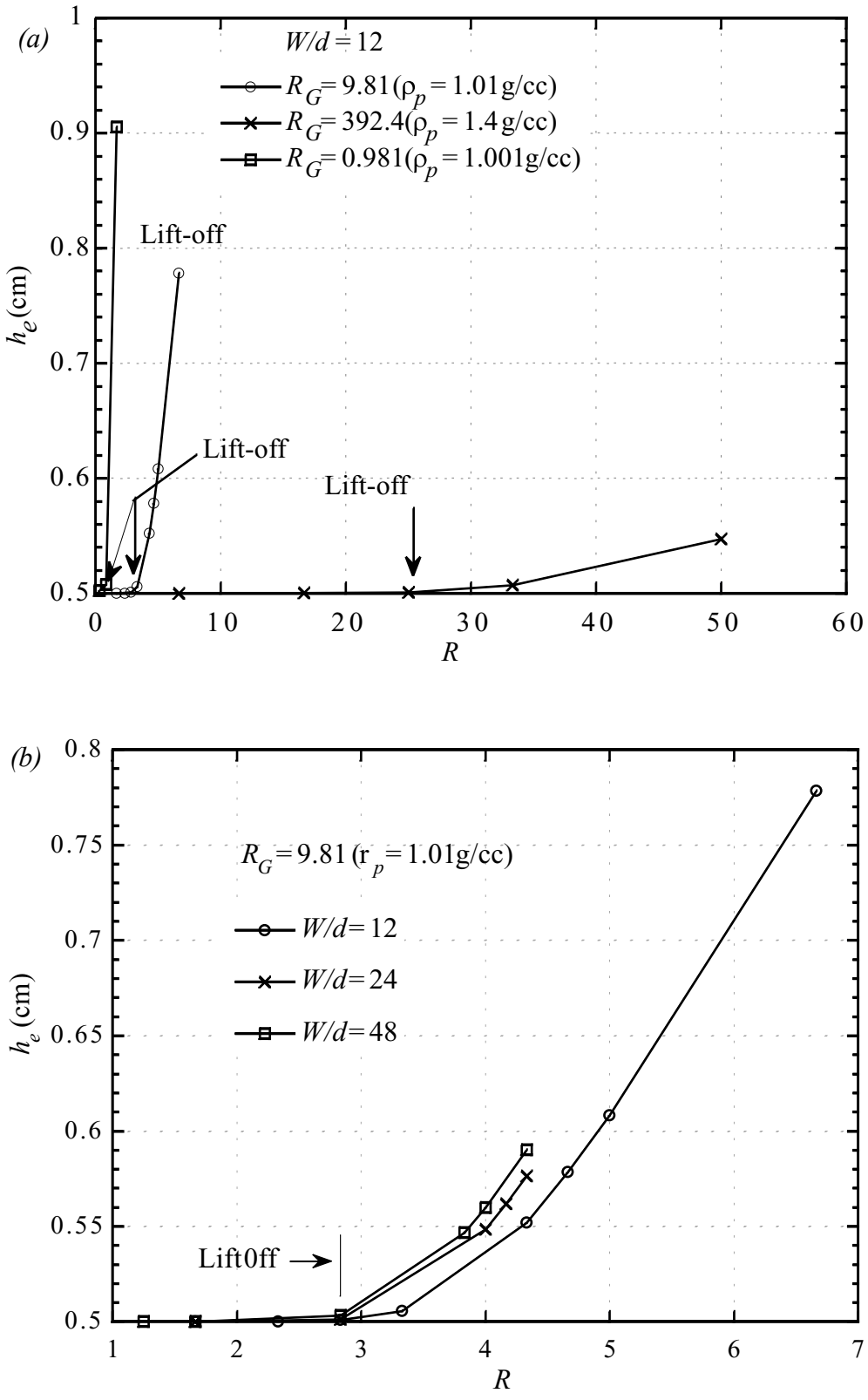

Figure IX.4 (a) Lift-off and equilibrium height as a function of the shear Reynolds number at different values of R_G. *(b) Equilibrium height vs. shear Reynolds number at different channel widths.*

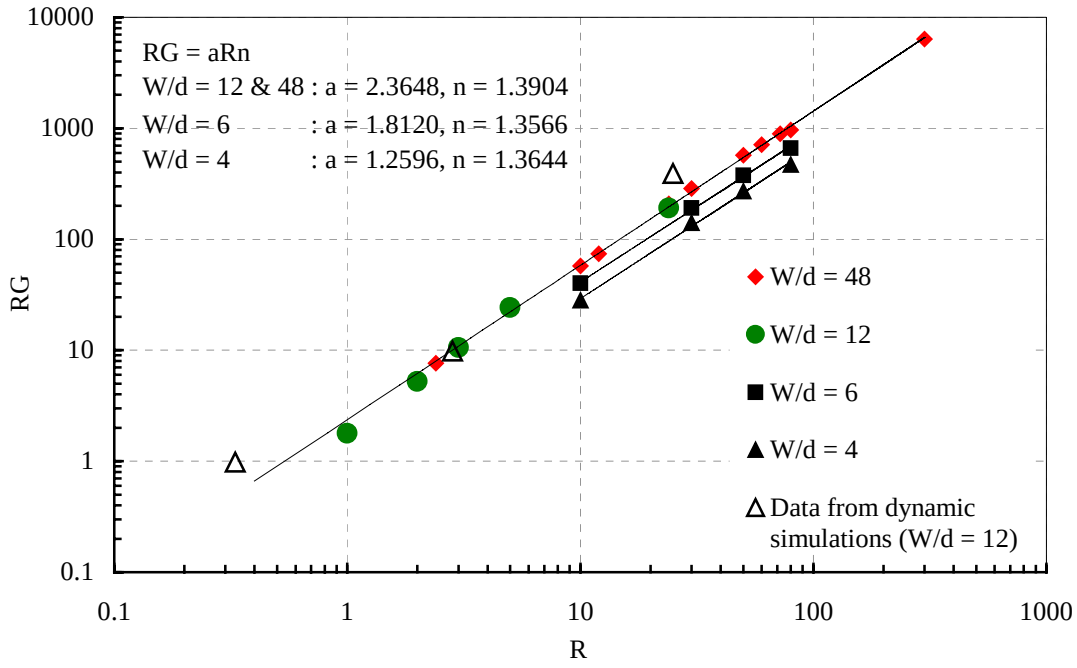

Figure IX.5. The plot of R_G *vs. the critical shear Reynolds number* R *for lift-off on a logarithmic scale at different values of* W/d.

We did many simulations of lift-off from the height 0.501*d*, varying *R* and *W/d*, and post processed the results in terms of *R* and R_G (see figure IX.5). The particle moves only under forces of the fluid motion and gravity; no axial force or torque is applied. Figure IX.5 shows the plot of R_G vs *R* at different values of *W/d*; a larger *R* is required to elevate heavier particle. The channel width apparently does not influence the correlation when *W/d* > 12 (figures IX.4 and IX.5). The data for *W/d* > 12 collapse onto the power law curve

$$R_G \approx 2.36\, R^{1.39} \qquad \text{(IX.17)}$$

This may be the first correlation obtained from numerical experiments, based on DNS and it points to one future direction for interrogation of DNS.

U_p and Ω_p are the translational and angular velocities, respectively, of the particle in equilibrium when the particle accelerations vanish. In figure IX.6 we plot the results of dynamic simulations, the slip velocity, $U_f - U_p$ vs. equilibrium height for particles of different densities. A similar plot for the slip angular velocity, $\dot{\gamma}/2 - \Omega_p$, is shown in figure IX.7. A larger slip velocity is required at a given equilibrium height to balance a heavier particle.

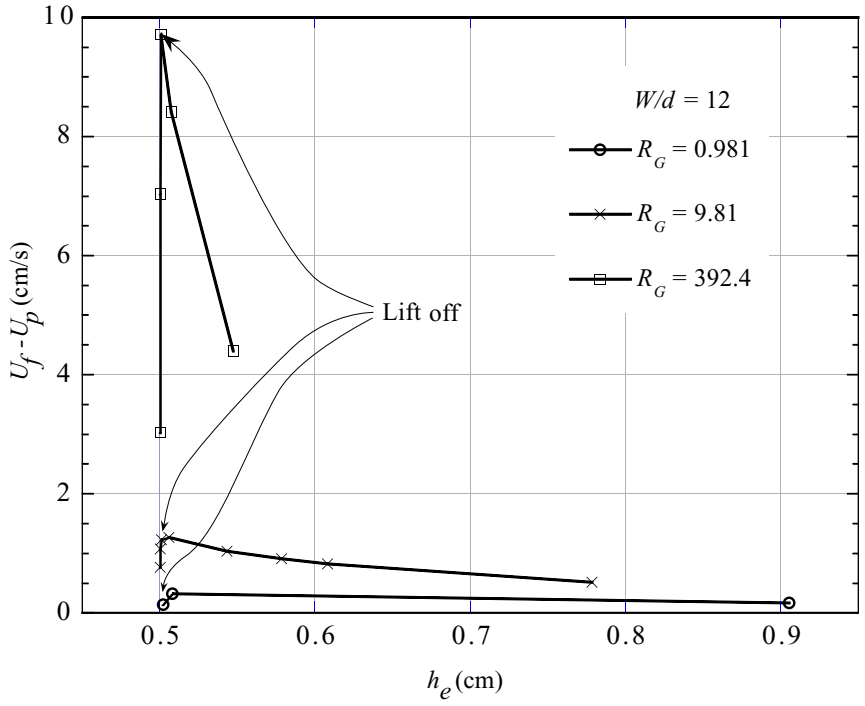

Figure IX.6. Slip velocity vs. equilibrium height for different particle densities.

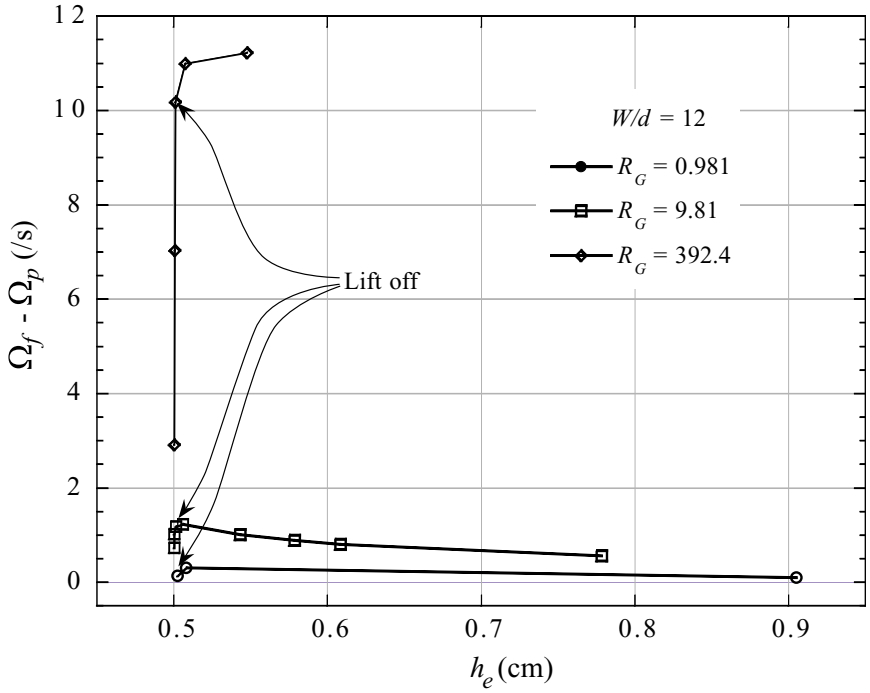

Figure IX.7. Slip angular velocity vs. equilibrium height for different particle densities.

In table IX.1 we have listed all the computed values of R_G, R/G, R, $\bar{p}$, h_e, U_p, U_f , $U_s = U_f - U_p$, Ω_p, $\Omega_f = \dot{\gamma}/2$ and $\Omega_s = \dot{\gamma}/2 - \Omega_p$ at equilibrium, where U_f and $\dot{\gamma}$ are as shown in figure IX.1.

The aforementioned quantities define a data structure generated by DNS which can be used to help in the creation and validation of lift models; the tables give the answers to which the models aspire.

*Table IX.1. Data structure for a freely translating and rotating circular particle levitated by Poiseuille flow (*d = *1 cm,* ρ_f = *1 g/cc and* η = *1 poise). Bold numbers represent the critical condition for lift-off. All the dimensional variables are given in CGS units. (a)* W/d = *12,* L/d = *22, (b)* W/d = *24,* L/d = *44, (c)* W/d = *48,* L/d = *88.*

Table IX.1a

R/G	R_G	R	$\overline{p}$	h_e	U_p	U_f	U_s	Ω_p	Ω_f	Ω_s
0.1133	**0.981**	**0.3333**	**0.0555**	**0.5024**	**0.0170**	**0.1605**	**0.1436**	**0.0161**	**0.1527**	**0.1367**
0.7079	0.981	0.8333	0.1389	0.5081	0.0820	0.4055	0.3235	0.0752	0.3814	0.3062
2.8316	0.981	1.6667	0.2778	0.9055	1.2310	1.3953	0.1643	0.6085	0.7076	0.0991
0.8183	**9.81**	**2.8333**	**0.4722**	**0.5012**	**0.1337**	**1.3608**	**1.2271**	**0.1147**	**1.2983**	**1.1836**
1.1326	9.81	3.3333	0.5556	0.5058	0.3479	1.6149	1.2670	0.2934	1.5262	1.2328
1.7697	9.81	4.1667	0.6944	0.5433	1.1230	2.1613	1.0383	0.8868	1.8947	1.0079
2.2200	9.81	4.6667	0.7778	0.5786	1.6560	2.5699	0.9139	1.2220	2.1083	0.8863
2.5484	9.81	5.0000	0.8333	0.6083	2.0590	2.8873	0.8283	1.4430	2.2465	0.8035
4.5305	9.81	6.6667	1.1111	0.7784	4.3350	4.8527	0.5177	2.3340	2.9009	0.5669
1.5928	**392.4**	**25.000**	**4.1667**	**0.5009**	**2.2820**	**11.999**	**9.7178**	**1.2790**	**11.456**	**10.177**
2.8316	392.4	33.333	5.5556	0.5074	7.7790	16.198	8.4192	4.2600	15.257	10.997
6.3710	392.4	50.000	8.3333	0.5475	21.730	26.126	4.3960	11.500	22.719	11.219

Table IX.1b

R/G	R_G	R	$\overline{p}$	h_e	U_p	U_f	U_s	Ω_p	Ω_f	Ω_s
0.8183	**9.81**	**2.8333**	**0.2361**	**0.5015**	**0.1611**	**1.3912**	**1.2301**	**0.1381**	**1.3575**	**1.2194**
1.6310	9.81	4.0000	0.3333	0.5485	1.2020	2.1439	0.9419	0.9468	1.9086	0.9618
1.7697	9.81	4.1667	0.3472	0.5619	1.3990	2.2864	0.8874	1.0750	1.9858	0.9108
1.9141	9.81	4.3333	0.3611	0.5766	1.6030	2.4386	0.8356	1.2010	2.0626	0.8616

Table IX.1c

R/G	R_G	R	$\overline{p}$	h_e	U_p	U_f	U_s	Ω_p	Ω_f	Ω_s
0.8183	**9.81**	**2.8333**	**0.1181**	**0.5034**	**0.2491**	**1.4113**	**1.1622**	**0.2134**	**1.3870**	**1.1736**
1.4979	9.81	3.8333	0.1597	0.5467	1.1640	2.0718	0.9078	0.9247	1.8730	0.9483
1.6310	9.81	4.0000	0.1667	0.5600	1.3590	2.2139	0.8549	1.0540	1.9533	0.8993
1.9141	9.81	4.3333	0.1806	0.5901	1.7750	2.5257	0.7507	1.3070	2.1134	0.8064

▪ Data Structure for DNS and experiments

We have identified two distinguished regimes: lift-off and equilibrium. For lift-off we would like to know

i. The critical condition for lift-off (the pressure gradient, Reynolds or other prescribed control parameter)

ii. The particle velocity U_p at criticality

iii. The particle angular velocity at criticality

iv. The velocity and shear rate at the particle center when there is no particle present

v. The slip velocity and slip angular velocity at criticality

At equilibrium we have a similar list. At equilibrium we wish to know

h_e	(height of mass center at equilibrium)
U_p	at h_e
U_f	at h_e
Ω_p	at h_e
$\dot{\gamma}/2$	at h_e
$U_f - U_p$	at h_e
$\dot{\gamma}/2 + \Omega_p$	at h_e

The aforementioned quantities define a data structure for DNS, which may be used to develop a theory of fluidization by lift. Tables IX.1 and IX.2 show how to structure data from DNS to test certain modeling assumptions. Plots of the rise evolution of neutrally buoyant particles are given in figures IX.8 and IX.9. The neutrally buoyant particles rise rapidly, reaching an equilibrium value not determined by the buoyant weight, in this case the equilibrium height *he* is the place where the lift vanishes. The generation of zero lift for a neutrally buoyant particle is associated with the curvature of the velocity profile in Poiseuille flow. The freely rotating particle with R = 5.4 rises to a distance of 2.248 cm from the center of the channel as compared to 3.6 cm from the center which is the "Segré-Silberberg" radius (0.6 w/2). The nonrotating particle rises further to 4.999 cm. The heavy particle $\rho_p = 1.01$ also rises further when the free rotation is suppressed and R = 16.2, but the rise of freely rotating and nonrotating heavy particles is not greatly different when R = 5.4. It may be true that models, which ignore particle rotation will overestimate lift.

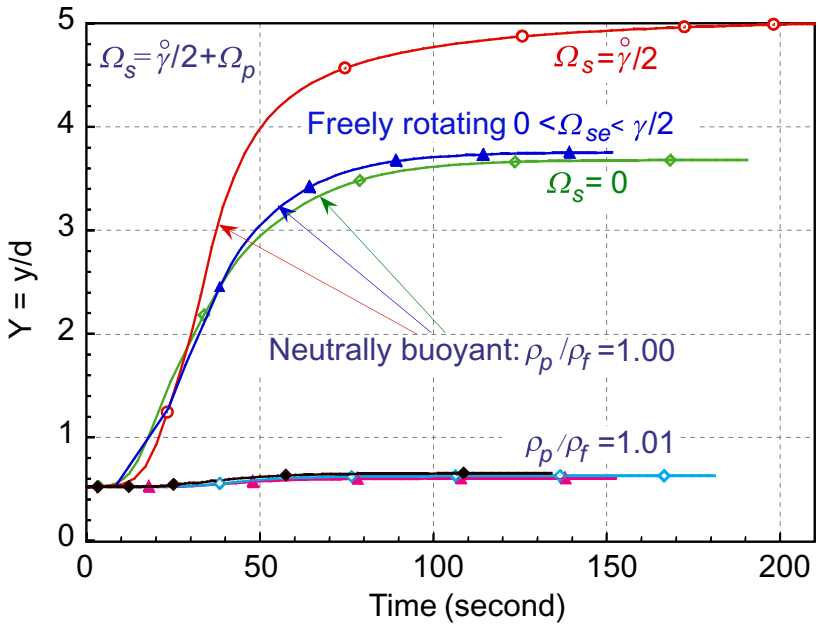

Figure IX.8 *Rise vs. time for R_w = 5.4. Compare rise of freely rotating and nonrotating particles. Nonrotating ones rise more. A neutrally buoyant, freely rotating particle rises closer to the center line than the "Segré-Silberberg" experiment; the nonrotating one rises even more. Models which ignore particle rotation overestimate lift. A yet smaller lift is obtained when the slip velocity is entirely suppressed (Ω_s = 0), but the particle does rise. The greater the slip velocity, the higher the particle will rise.*

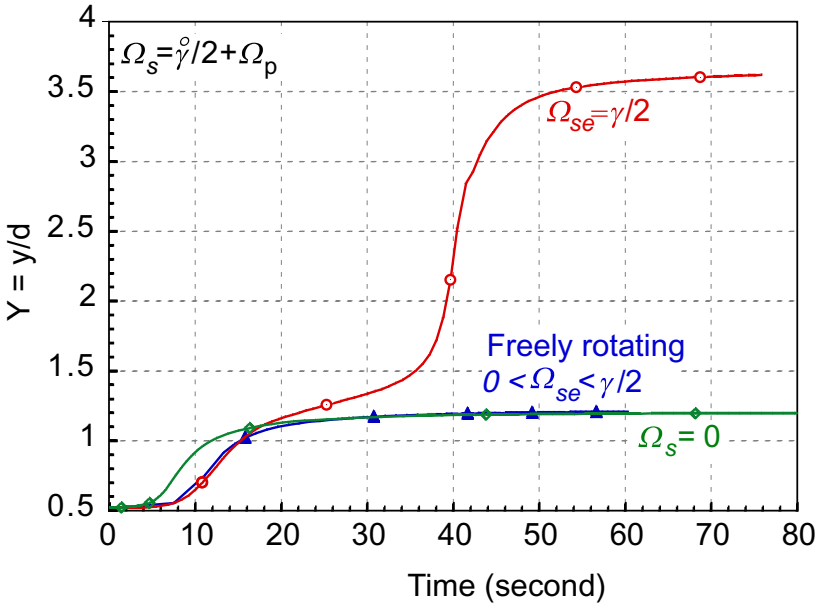

Figure IX.9 *Rise vs. time for a circular particle ρ_p/ρ_f = 1.01 when $R_w = \dot{\gamma}_w d^2/\eta = 16.2$. The rise of the particle is an increasing function of the slip velocity in the range $0 \le \Omega_s \le \dot{\gamma}/2$ and is a maximum when the particle velocity is suppressed. The freely rotating particle has a small positive slip angular velocity.*

There are a small number of experiments on the inertial lift of single particles. The data obtained falls far short of that necessary for testing ideas about lift-off and levitation to equilibrium. The list of quantities mentioned at the head of this section as well as data on stability and bifurcation are not adequately probed in these experiments; more penetrating experiments should be done.

*Table IX.2 Data structure for a circular particle levitated by Poiseuille flow (*W/d *= 12,* L/d *= 22,* d *= 1cm,* η *= 1 poise). The data for steady flow after the particles rises to its equilibrium height. Three cases are considered:* $\Omega_p = 0$*, freely rotating (*) and* $\Omega_s = 0$*.*

ρ_p/ρ_f	Re	h_e (cm)	Ω_p (sec^{-1})	U_p (cm/sec)	$\dot{\gamma}/2$ (sec^{-1})	$u_f = \dot{\gamma} h_e$ (cm/sec)	Ω_{slip} (sec^{-1})	U_{slip} (cm/sec)
1.00	5.4	4.999	0.0	15.670	0.450	15.749	0.450	0.080
*1.00	5.4	3.753	0.958	13.780	1.011	13.928	0.053	0.148
1.01	5.4	0.681	1.044	13.630	1.044	13.780	0.0	0.150
1.01	5.4	0.602	0.0	2.125	2.429	3.088	2.429	0.963
*1.01	5.4	0.627	1.560	2.296	2.418	3.208	0.858	0.912
1.01	5.4	0.651	2.407	2.453	2.407	3.325	0.0	0.872
1.01	16.2	3.620	0.0	40.260	3.213	40.953	3.213	0.693
*1.01	16.2	1.211	5.320	17.410	6.465	17.638	1.145	0.228
1.01	16.2	1.199	6.481	17.190	6.481	17.483	0.0	0.293

Eichhorn and Small 1964 suspended a small sphere in Poiseuille flow through an incline tube and determined the lift and drag coefficients on the particle. By suspending the sphere in the flow, the lift and drag forces are calculated from the tangential and normal components of the buoyancy force with the flow. The results are not extensive, but at the time did provide new information about the drag and lift on spheres in such flows. These experiments showed that the lift coefficient increases with Reynolds number. However, the accuracy of the measurements was limited and the variables such as rotation speed and radial position are related by the operating characteristics of the apparatus and could not be varied independently.

Bagnold 1974 measured the lift and drag forces on spheres and cylinders in the gravity flow of a liquid in an open channel (the upper, free boundary of the liquid is frictionless). The objects are placed near the lower, solid boundary of the device and are allowed to translate down the channel in the shear flow. Bagnold overcame the problem of the limited channel length by creating a stationary "flow" where the lower boundary is replaced with an endless belt that translates in the direction opposite the free stream velocity. By producing the proper flow kinematics to balance the inertial motion of the sphere down the channel, the particle can be suspended in the flow and the equilibrium height can be measured. In separate measurements, a linkage assembly is used to measure the drag and lift forces on bodies fixed in the flow field. In general, Bagnold observed that the lift force decreases rapidly with increasing distance from the solid boundary and disappears when the clearance exceeds on particle diameter. Unfortunately, the author admits, "the experiments must be regarded as exploratory only" because of the accuracy of the device and the limited scope of the experiments.

Cherukat, McLaughlin and Graham 1994 used a homogeneous shear flow apparatus (HFA) to measure the shear-induced inertial lift on a rigid sphere. The HFA device creates a uniform linear shear flow between two timing belts moving in opposite directions. Spheres were injected onto the mid-plane between the two belts will translate between the belts, migrating laterally towards one of the walls. A system of cameras recorded the motion of the particle that was then used to calculated the dimensionless lift force on the sphere. The lift force increases with the ratio of $\varepsilon = \sqrt{\mathrm{Re}}/\mathrm{Re}_s$, where Re is the shear Reynolds number of the flow and Re_s is the Reynolds number of the sphere based on the slip velocity. These results, within experimental error, validated the theory of McLaughlin 1991 and they showed that Saffman's expression overpredicts the lift if $\varepsilon >> 1$. However, these experiments are not able to measure the equilibrium height from the wall, and the rotation velocity of the sphere is not presented.

Experiments by Mollinger and Nieuwstadt 1996 examined the lift forces on particles within the viscous sublayer of highly turbulent flows (Re ~ 10^6). Their experimental device measures the lift force on a small particle permanently affixed to cantilever beam at the surface over which air flows in a wind tunnel. Optical methods allow for measuring the lift force to an accuracy of 10^{-9} N. Their results show a substantial difference between experiments and theory for this regime of Reynolds numbers. However, because the particle is fixed onto the surface, measurements of important parameters such as equilibrium height, slip velocity, and rotation rate are unobtainable.

Ye and Roco 1992 measured the velocity and angular velocity for neutrally buoyant spheres with diameters from 3 to 8 cm in a plane turbulent Couette flow at three shear rates corresponding to Reynolds number (4.6, 6.8, 9.2) $\times 10^4$. Fluid and particles were assumed to have the same velocity; slip velocities were not measured. Particle spin increases rapidly near the walls. No significant differences between the angular velocity of 6.36 and 7.94mm spheres were found, but smaller spheres of 4.76 and 3mm rotate faster.

More recently, King and Leighton 1997 used a rotating parallel-plate device to measure translation velocity and the angular velocity of particles in contact with a wall. The velocities were determined by timing the particle as it travels through an arc length. A wide range of Reynolds numbers could be sampled because the local shear rate between the parallel plates is proportional to the radial distance. Unfortunately, secondary currents drive the particle inwards at larger Reynolds numbers. This study showed that the particle undergoes three different modes of motion as the flow Reynolds number is increased: (i) solid body rotation along the wall, (ii) particle rotation with translational slip along the wall, and (iii) translation and rotation in the free stream following lift-off. Careful attention was paid to the surface roughness of the sphere and the frictional coefficient of the wall that plays an important role in the motion when the sphere is in contact with the wall. The transition from (i) to (ii) was observed to scale with $\mathrm{Re}/\mathrm{Re}_s$ ~ 0.1; while lift-off occurred when $\mathrm{Re}^2/\mathrm{Re}_s$ ~ 4. These experiments were in good agreement with the rough sphere model proposed by Krishnan and Leighton 1995 for a range of reasonable surface roughness values. No values of the equilibrium height were presented.

It is more difficult to specify a data structure for interrogating DNS for the modeling of lift on particles in a flowing suspension in pipes and conduits in which hydrodynamic interactions are important. At present there are no satisfactory models for this problem. Perhaps an approach to this modeling can be developed along the lines followed by Richardson and Zaki. In their case it was necessary to find an empirical formula for the slip velocity in a suspension in the factored

form (VI.60), the product of the terminal or blow-out velocity for a single particle with the hindered settling function. We have shown that such an empirical relation can be formed from data from DNS. All the factors in (VI.60) are empirical; analytical formulas for the terminal velocity are known only for low Reynolds number flow, Stokes and Oseen flows. It is almost certain that role of first principle formulas from analysis is even more limited in the problem of lift.

The Richardson-Zaki experience teaches also that the existence of a good correlation like (VI.16) does not automatically lead to a drag formula; creative intelligence is still required.

To arrive at an appropriate data structure for lift in suspension it is necessary to identify what quantifies ought to be modeled and how these quantities enter into models for lift. For example, we can consider that idea that lift formulas ought to depend on the slip and angular slip velocities and seek these in a factored form, products of slip and angular slip velocity for a single particle with to-be-determined hindered settling functions. To see what may be involved in an approach like this it is instructive to search for ideas in the very restricted situations for which mathematical analysis is possible.

X Analytical models of lift

We have already noted that the domain of parameters for which mathematical analysis is possible is rather severely restricted. As in the case of fluidization by drag, the analysis is mainly restricted to Stokes and Oseen flow Reynolds number drag and rather overly complicated analysis of perturbation of these with inertia. The main problem with the perturbations is that the Stokes flow is not uniformly valid, for away from the body inertia and viscosity are both important and rather complicated analysis involving the matched asymptotic expansions must be involved. The low Reynolds number far lift from a wall is slightly different, because if the particle is heavy and not lifted too far away from wall, regular rather than singular perturbations can be used. Another difference between lift and drag is that you get fine lift formulas in 2D with viscosity completely neglected as in aerodynamic theory; no such formulas can be obtained for drag.

Our goal here is to explore some ways DNS can be used to generate engineering models of lift which almost always have an empirical input, as does the Richardson-Zaki theory. It is to be hoped that DNS is a source for the empirical input. To achieve our goal we must first come to realize what quantities will enter into expressions for lift in a slurry. For a single particle, say a sphere, we would like to understand the role of fluid shear and shear gradients (curvature), particle velocity and angular velocity, wall effects and fluid material parameters. The brief discussion of analytical results to follow focuses on how these quantities enter into lift in the rather special cases in which lift formulas can be written down. These formulas are compositions of the quantities listed in tables IX.1 and IX.2 and in similar to-be-created tables for levitating spheres, and they can be evaluated and generalized by DNS.

The lift on a particle moving forward is a force opposing gravity perpendicular to the motion. More generally we may identify the lift as the component of a force transverse to the motion in the direction of gravity.

▪ Lift in an inviscid fluid

First we can look on formulas in a fluid without viscosity for which viscous drag is impossible. The most famous formula for lift on a body of arbitrary shape moving forward with velocity U in a potential flow with circulation Γ was given by

$$L' = \rho U \Gamma \tag{X.1}$$

where ρ is the fluid velocity and L' is the lift per unit length.

The lift on circular cylinder of radius a is of special interest. A viscous potential flow solution for a stationary cylinder rotating with velocity Ω which satisfies the no slip boundary is given by

$$\mathbf{U}(r) = \mathbf{e}_\theta \Omega a^2 / r, \quad \mathbf{u}(a) = \mathbf{e}_\theta \Omega a \tag{X.2}$$

The circulation for this viscous potential flow is

$$\Gamma = \oint \mathbf{u} \bullet dx = 2\pi\Omega a^2 \tag{X.3}$$

When this rotating cylinder moves forward it generates a lift L' per unit length

$$L' = 2\pi\rho a^2 U\Omega \tag{X.4}$$

The direction of the lift can be determined by noting that the velocity due to rotation adds to the forward motion of the cylinder at the top or bottom of the rotating cylinder according to the directions of Ω and U. In figure X.1 the velocity is smaller on the bottom of the cylinder; by the Bernoulli equation, the pressure is greater there and it pushes the cylinder up.

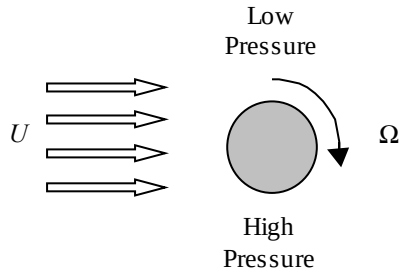

Figure X.1 The lift per unit length $L' = 2\pi\rho a^2 U\Omega$ on a cylinder of radius moving forward at speed U and rotating with velocity Ω in such a way as to reduce the velocity at the bottom and add at the top.

The effect of proximity to the ground is enhanced lift. An aerodynamic formula for this can be derived by the method of reflections, representing the airfoil by a point vortex (see, e.g. Kuethe and Chow 1998).

$$L' = \rho U\Gamma\left[1+\frac{c}{16h^2}-\frac{\Gamma}{4hU}\left(1+\frac{c^2}{16h^2}\right)\right] \tag{X.5}$$

where c is the chord and h the distance of the vortex from. We can write a ground effect formula for the lifting of a cylinder by putting $c = 2a,\ \Gamma = 2\pi\Omega a^2$; the

$$L' = 2\pi\rho a^2 U\Omega\left[1+\frac{a}{8h^2}-\frac{\pi\Omega a^2}{2hU}\left(1+\frac{a^2}{4h^2}\right)\right]. \tag{X.6}$$

If U and Ω are given we could compute h from the balance of buoyant weight and lift $L' = \pi a^2(\rho_p - \rho)g$.

Another formula for the lift of on particle in an inviscid fluid in which uniform motion is perturbed by a weak shear was derived by Auton 1987 and a more recent satisfying derivation of the same result was given by Drew and Passman 1999. They find that

$$L = \frac{2}{3}\pi a^3 \rho\,\boldsymbol{\omega} \wedge (\mathbf{u} - \mathbf{U}) \tag{X.7}$$

for the lift force on sphere of radius a. In plane flow $\boldsymbol{\omega} = \mathbf{e}_z \overset{\circ}{\gamma},\ \mathbf{u} - \mathbf{U} = \mathbf{e}_x(u - U)$, gravity is $\mathbf{g} = -g\mathbf{e}_y\gamma = -g(\mathbf{e}_x \wedge \mathbf{e}_z)$, we have

$$L = -\frac{4}{3}\pi a^3 \rho \Omega_f (u - U)\mathbf{e}_y \tag{X.8}$$

where

$$2\Omega_f = -\dot{\gamma} = -du/dy . \tag{X.9}$$

If $du/dy > 0$ the sphere is lifted against gravity when the slip velocity $u - U$ is positive; if $u - U$ is negative the sphere will fall. Particles which lag the fluid migrate to streamlines with faster flow, particles which lead the fluid migrate to streamlines with slower flow.

There are rather striking differences between (X.8) and (X.4); first (X.4) depends on the angular velocity of the particle but (X.8) depends on the angular velocity of the fluid. Both formulas leave the slip velocity undetermined, $u - U$ appears in (X.8) because of the shear, in (X.4), $u = 0$. The slip velocities have to be prescribed in these theories because the particle velocity is not determined by viscous drag. Similarly the angular velocity of the particle cannot arise from torques arising from viscous shears. The effects of particle rotation cannot be obtained by the method of Auton 1987.

▪ Low Reynolds numbers

Other lift formulas have been obtained in the limit of low Reynolds numbers. Inertial effects are much smaller than viscous effects near a slowly moving particle, but these effects are comparable far away from the particle. This non-uniformity generates mathematical difficulties, which are especially severe for perturbations; different regimes of flow must be distinguished and different cases arise. We shall not present a review of these difficulties in detail; extended discussion of the subtle problems arising in discussions of lift at low Reynolds number have been presented by Brenner 1966, Cox & Mason 1971, Leal 1980, Feuillebois 1989, Cherukat and McLaughlin 1994, and Asmolov 1999, among others. The review of the literature given in the DNS study of migrations of particles in plane Couette and Poiseuille flow is of value since it compares analytical studies of migration with restricted domains of validity with direct numerical solutions of similar problems when the restrictions are relieved.

In unbounded domains Stokes flow is not uniformly valid even though the celebrated Stokes flow solution giving the drag on a sphere is an achievement of enormous utility. The problem becomes evident when one perturbs this solution with small inertia to correct the drag. The perturbation in powers of the Reynolds number (inertia) fails because there are important effects of inertia in the far field at lowest order which are not present in Stokes flow. The same problem has even stronger consequence in plane flow; there is no bounded Stokes flow for flow over a body.

Oseen solutions of the Navier-Stokes equations linearized for uniform flow over a body can be obtained and matched with the Stokes solution near the body by methods of matched asymptotic expansions. This leads to a correction of Stokes drag for flow over a sphere in three dimensions; in two dimensions the method of matched asymptotic using Oseen's solution gives a low Reynolds number solution in the case where Stokes flow fails.

The same problem of perturbing Stokes flow for corrections of drag occur when perturbing Stokes flow for lift; on unbounded domains it is necessary to turn to matched asymptotic solutions.

It is essential to understand that Stokes flows will not generate lift; to get lift from the Navier-Stokes equations some effects of inertia must be considered. Saffman 1956 and Bretherton 1962 showed that no sideways force on a single rigid spherical particle can be derived from Stokes equations whatever the velocity profile and relative size of particle and tube if the velocity is unidirectional.

We turn now to some studies of lift in low Reynolds number flows on unbounded domains obtained by matching inertialess solutions near a body to Oseen's solution far away. Those cases could be considered; uniform flow flows with a uniform shear, like Couette flow, and flows like Poiseuille flow with a shear gradient. Rubinow and Keller (RK) 1961 derived a formula for the transverse force on a spinning sphere in a viscous fluid which is at rest at infinity, at low $R = Ua/\nu$

$$L = \pi a^3 \rho \, \mathbf{\Omega} \wedge \mathbf{U}\big(1 + O(\mathrm{Re})\big). \tag{X.10}$$

If $\mathbf{\Omega}$ and $\mathbf{U}$ are orthogonal, (X.10) reduces

$$L = \rho \pi a^3 U \Omega . \tag{X.11}$$

In RK's problem the velocity U of the sphere and Ω its angular velocity are maintained by an external agent and a drag and torque may be computed.

The forms of (IX.1) and (X.11) are identical apart from a prefactor despite the fact that (IX.1) is for two dimensions in the flow of an inviscid fluid and (X.11) is for a sphere in a highly viscous (low R) flow. The ratio $L/L' = a/2$ differs by $a/6$ from the ratio of the volume to the perimeter of a sphere.

The RK lift (X.11) also differs from Auton's 1987 lift (X.7) in several ways: the prefactor in (X.7) is 4/3 times that in (X.11); (X.11) is for uniform flow and (X.7) for shear flow; (X.11) is for low and (X.7) for high Reynolds number with no viscous effects; and RK lift depends on the spin of the particle but Auton's lift depends on the "spin" Ω_f of the fluid. Apart from these gigantic differences the formulas look alike. We might ask when the particle spin, the fluid spin or the difference $\Omega_f - \Omega$ is most important. This comparison brings out the importance of the way in which the measure of angular velocity enters into lift; we could look at the difference of lift when the particle rotates freely and when the particle rotation is suppressed. In figure IX.9 we show that a heavier than liquid cylinder will rise higher when rotation is suppressed than when it rotates freely, and table IX.2 shows that the slip angular velocity is greatly reduced when the particle rotates freely.

Application of Auton's formula (X.7) to a real situation could overestimate the lift due to the fact that the angular velocity of the particle cannot adjust to the shear stresses which are generated by shear at the particle surface in a viscous fluid.

▪ Lift in shear flows at low *R*

The experiments of Segré and Silberberg 1961, 1962 have had a big influence on fluid mechanics studies of migration and lift. They studied the migration of dilute suspensions of neutrally buoyant spheres in pipe flows at Reynolds numbers between 2 and 700. The particles migrate away from the wall and centerline and accumulate at 0.6 of a pipe radius.

Rubinow and Keller 1961 discussed the aforementioned experiments and tried to apply their lift theory to explain the observations. They remark that their theory is for a sphere in a uniform flow but the Poiseuille flow in a tube is not uniform; it is a shear flow with a parabolic profile. They say that the shear accounts for the spin and the shear gradient accounts for the lag.

Bretherton 1962 considered the lift and drag force on a cylinder (2D sphere) and Saffman 1965 the lift force on a sphere in an unbounded shear flow. They matched Stokes flow near the body to Oseen flow far away. Bretherton found that the lift and drag per unit length at small values of $R = \dot{\gamma} a^2 / \nu$ is given by

$$L' = \frac{21.16 \eta U_s}{\left(0.679 - \ln\left(\sqrt{R/4}\right)\right)^2 + 0.634}, \qquad D' = \frac{4\pi\eta U_s \left(0.91 - \ln\left(\sqrt{R/4}\right)\right)}{\left(0.679 - \ln\left(\sqrt{R/4}\right)\right)^2 + 0.634}, \tag{X.12}$$

where U_s is the slip velocity, η the viscosity, $\nu = \eta/\rho$. Saffman 1965 found that the lift on a sphere in a linear shear flow is given by

$$L = 6.46 \eta a^2 U_s (\overset{\circ}{\gamma}/\nu)^{1/2} + \text{lower order terms}. \tag{X.13}$$

The lower order terms are

$$-U_s a^3 \rho_f + \left[\frac{11}{8}\overset{\circ}{\gamma} - \pi\Omega\right] = -U_s a^3 \rho_f \left[-\frac{11}{4}\Omega_f - \pi\Omega\right] \tag{X.14}$$

and they are lower order as $\nu \to \infty$ for small *R*. When $U_s > 0$ the sign of the first term is positive when $\dot{\gamma} > 0$, negative when $\dot{\gamma} < 0$; assuming that $\dot{\gamma} > 0$, the lift is positive when $U_s > 0$ and negative when $U_s < 0$. The lower order terms depend strongly on the slip angular velocity Ω_p - $\Omega_p = \Omega_p + \dot{\gamma}/2$. Saffman's result requires that the particle Reynolds number based on the slip velocity is small $2U_s a/\nu << 1$ and the flow Reynolds number $R = \dot{\gamma} a^2 / \nu$ is small and another restrictive condition which was removed by McLaughlin 1991 and Asmolov 1990.

These results cannot explain Segré-Silberberg's observations, which require migration away from both the wall and the center. There is nothing in these formulas to account for the migration reversal near 0.6 of a radius. Moreover the slip velocity U_s and angular slip velocity which are functionals of the solution are prescribed in these studies.

▪ Slip velocity and lift

A definite value for the slip velocity may be obtained by preventing lateral migration by balancing the hydrodynamic lift with the buoyant weight of the particle. Applying this balance to (X.12) and (X.13) we get

$$U_s = \frac{\pi d^2 (\rho_p - \rho_f) g \left[\left(0.679 - \ln\left(\sqrt{R/4}\right)\right)^2 + 0.634 \right]}{84.63\eta} \quad \text{for a circular particle,}$$
$$U_s = \frac{\pi d^2 (\rho_p - \rho_f) g}{9.69\eta\sqrt{R}} \quad \text{for a sphere.} \tag{X.15}$$

The net buoyant weight on a neutrally buoyant particle $(\rho_p = \rho_f)$ is zero; hence $U_s = 0$ and $L = 0$. The Bretherton and Saffman formulas thus predict that a freely moving neutrally buoyant circular or spherical particle will have zero slip velocity in a linear shear flow in an unbounded domain.

Lin, Peery and Schowalter 1970 did a low Reynolds number analysis of simple shear flow around a rigid sphere by matching Stokes and Oseen flow. They enforced the condition of no net force or torque and found that

$$U_s = 0,$$
$$\Omega_p = -\overset{\circ}{\gamma}\left(\frac{1}{2} - 0.153\delta R^{3/2}\right) \tag{X.16}$$

where $R = \dot{\gamma} a^2 / \nu$. This shows that the slip velocity in an unbounded linear shear flow vanishes but the angular slip velocity is proportional to $R^{3/2}$. Relaxing the assumption of small Reynolds numbers, Feng, Hu and Joseph 1994 did a direct simulation of a circular particle in plane Couette flow. They found that the particle migrates to center of the channel where it moves with the fluid but rotates at 46% of $\dot{\gamma}$ when the particle Reynolds number is about 0.63. Cox, Zia and Mason 1968 showed that the angular slip velocity vanishes for a freely moving and rotating particle in Stokes flow.

N. Patankar and Hu (Patankar 1997) gave a symmetry argument which suggests that spherical bodies which move with the fluid in a linear shear flow experience no lift even when they are not neutrally buoyant. This symmetry is displayed in figure X.6 where the imposed shear is represented in a coordinate system fixed at the shear center. The up-down symmetry implies that up-down lift are equally possible, hence the lift, and also the drag, is zero.

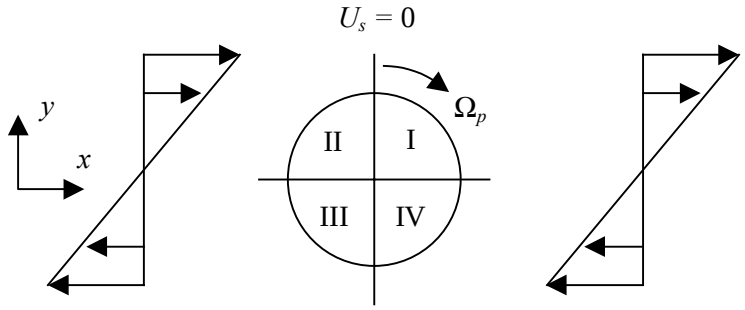

Figure X.6 A neutrally buoyant particle in an unbounded linear shear flow.

The symmetric $U_s = 0$ solution for a neutrally buoyant circular or spherical particle moving freely in an unbounded linear shear flow may be unstable under certain conditions not yet understood.

▪ Non-uniqueness

McLaughlin 1991 generalized Saffman's formula for lift; he found that

$$L = \frac{6.46}{2.255}\frac{\eta^2}{4\rho_f} R \frac{J(\varepsilon)}{\varepsilon}\,, \qquad \varepsilon = \frac{\sqrt{R}}{R_s}\,, \tag{X.17}$$

where J is a function of ε only and $R_s = \rho_f U_s d/\eta$ is the slip Reynolds number. The function J has a value of 2.255 as $\varepsilon \to \infty$ (the Saffman limit). Figure X.7 shows the plot of $J(\varepsilon)/\varepsilon$ as a function of ε (for $\varepsilon \geq 0.025$) based on the data provided by McLaughlin 1991. For a neutrally buoyant particle $J(\varepsilon)/\varepsilon = 0$ i.e. $\varepsilon = 0.218$ or $\varepsilon \sim \infty$ (figure X.7). There is probably another value of $\varepsilon < 0.025$ at which $J(\varepsilon)/\varepsilon = 0$ but we do not have that data. Equation (X.17) implies $U_s = \dfrac{\sqrt{R}\eta}{0.218\rho_f d}$ or $U_s = 0$ (prediction from the Saffman formula); hence the slip velocity is not single valued for a given L. The argument also works for non-neutrally buoyant particles. The two solutions of McLaughlin's equation may not both be stable.

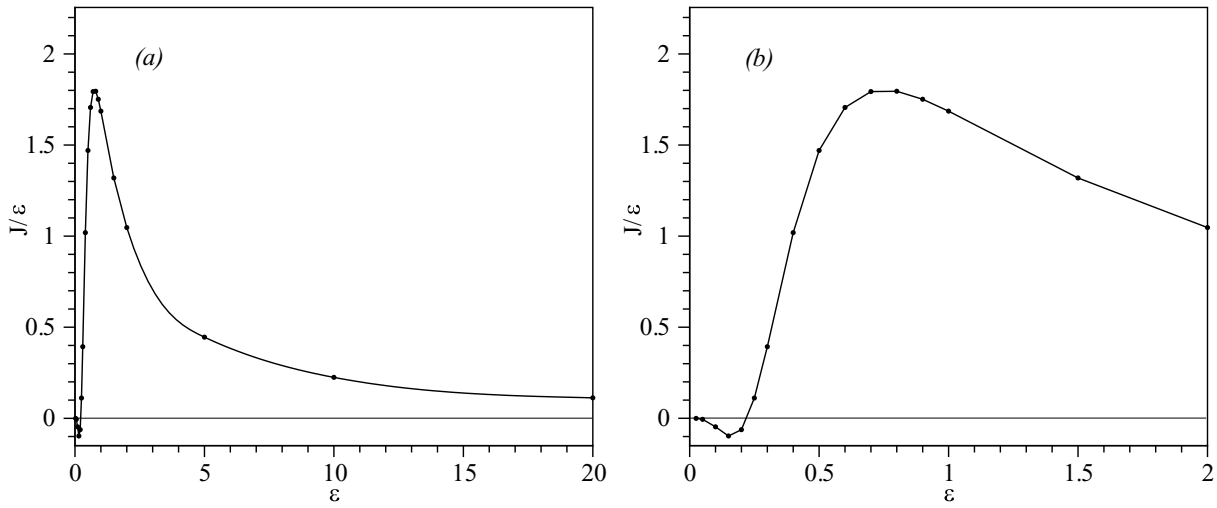

Figure X.7. Graphs of J(ε)/ ε *vs.* ε *for* ε > *0.025. The graphs are based on McLaughlin's data for the lift on a sphere in an unbounded linear shear flow.*

▪ Validation of lift formulas by DNS

An important application of DNS is to establish if and when analytic expressions for lift are valid. Most of the expressions found in the literature are for spheres and the formula will be tested in the future. An example of this kind of testing will now be given for Bretherton's formula's (X.12) for the lift and drag on a cylinder in a linear shear flow.

Bretherton's analysis does not apply to the case of a freely moving cylinder in equilibrium under the balance of weight and lift. The condition of zero drag, required for steady motion, is not respected. Assuming some engine to move the particle with the required drag, we may compare this formula with the results from DNS.

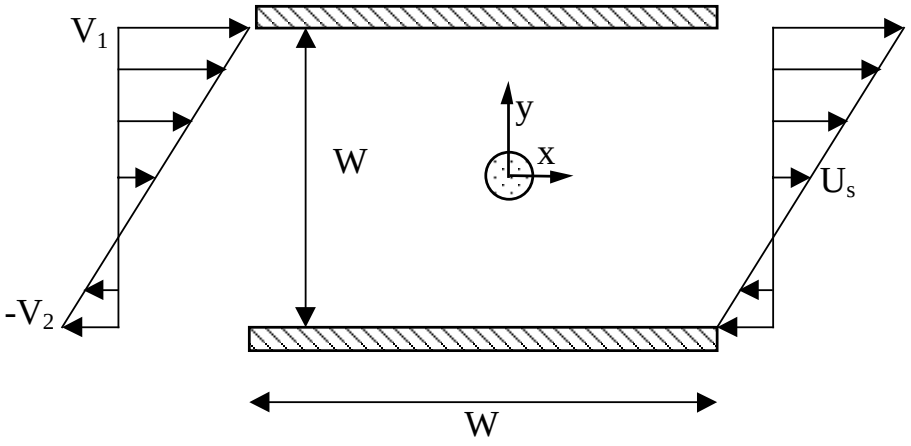

Figure X.8. Computational domain for the simulation of linear shear flows around a circular particle.

Numerical simulations were performed in a square channel of size $W \times W$. The channel size should be large enough to simulate flows in an unbounded domain. The circular particle was placed at the center of the channel and the coordinate system at the center of the particle. The velocity boundary conditions are as shown in figure X.8. The upper wall moves with velocity V_1

and the bottom wall with velocity -V_2. The shear-rate $\dot{\gamma} = (V_1 + V_2)/W$ and the slip velocity U_s is as shown in figure X.8. The particle is free to rotate so that the net torque is zero at steady state, and $\dot{\gamma}$ and U_s were varied in the simulation.

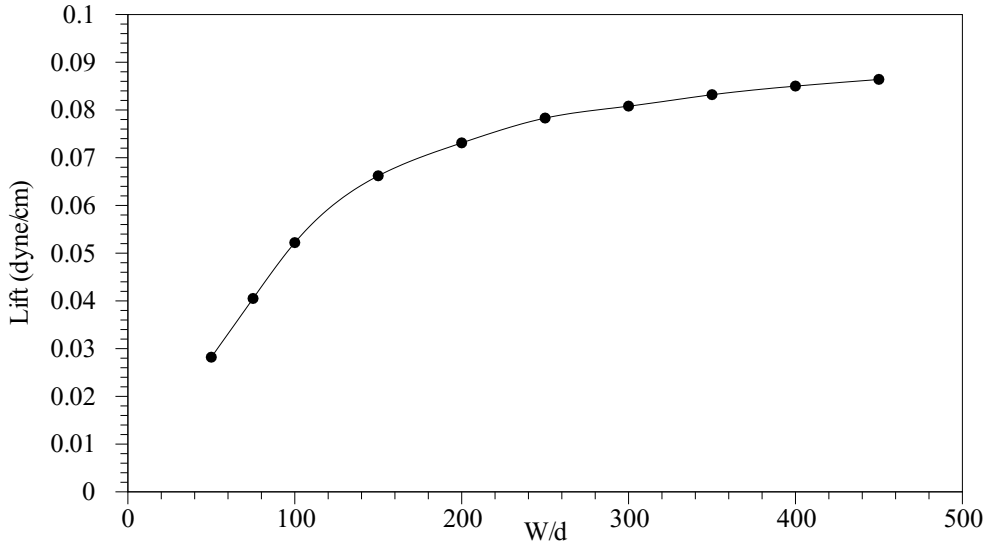

Figure X.9. Lift vs. domain size for a particle in an unbounded linear shear flow.

The fluid density is 1 g/cc, viscosity is 1 poise and the particle diameter is 1 cm. At $t = 0_+$ the flow is started by imposing the boundary conditions. The particle begins to rotate until a constant angular velocity is reached at steady state. The hydrodynamic lift (in the *y*-direction) and drag (in the *x*-direction) on the particle is calculated. Figure X.9 shows the plot of the lift force on the particle as a function of W for $R = 0.01$ and $R_s = 0.1$. The simulations were carried out on a sequence of domains of increasing size. If this procedure is to yield a result which is asymptotically independent of the size of the domain then the curve giving lift vs. domain size ought to flatten out. Figure X.9 shows just such a flattening. Though the curve is still rising modestly at W = 450d, we have used this domain for the simulations in table X.1. In this table the computed values of lift and drag are compared to the analytical values from Bretherton's expressions (X.12). The drag force is in better agreement than the lift. Larger domains may lead to better agreements.

		R_s = 0.003			**R_s = 0.1**		
		DNS	Analytic	% Error	DNS	Analytic	% Error
R = 0.01	Lift	0.00347	0.00449	-22.72	0.08593	0.1496	-42.56
	Drag	0.01010	0.01041	-2.98	0.3374	0.3471	-2.79
R = 0.02	Lift	0.00436	0.00542	-19.56	0.1239	0.1806	-31.39
	Drag	0.01093	0.01145	-4.54	0.3637	0.3818	-4.74

Table X.1. Comparison between the numerical and analytic values (equation X.12) of lift and drag per unit length (in CGS units). The error is calculated with respect to the analytic value.

▪ Wall effects in shear flows

(X.6) shows how the lift on a cylinder rotating the fluid in an aerodynamic approximation might be increased as it moves to the ground. A similar enhancement of lift in a shear flow near a wall occurred at low Reynolds numbers. The generation of lubrication layers in flowing suspensions is most probably a consequence of enhanced wall lift. The analysis of lift at low R is complicated by the non-uniform way in which viscosity and inertia enter the problem. A neighborhood $d_s > d$ of a sphere moving with a slip velocity U_s is dominated by viscous forces when

$$\mathrm{Re}\,(d_s, U_s) = \frac{U_s d_s}{\nu} << 1\,. \tag{X.18}$$

A neighborhood $l_w > 0$ of the wall in a shear flow is dominated by viscous forces when

$$\mathrm{Re}\,(l_w, \mathring{\gamma}) = \frac{\mathring{\gamma} l_w^2}{\nu} << 1\,. \tag{X.19}$$

The neighborhood $l > 0$ between the particle and the wall is dominated by viscous forces when

$$l < \min(d_s, l_w)\ . \tag{X.20}$$

The effect of inertia in this region dominated by viscosity enters as a perturbation of Stokes flow with terms arising from $\rho(\mathbf{u}\bullet\nabla)\mathbf{u}$, where $\mathbf{u}(\mathbf{x},t)$ is computed on Stokes flow. The perturbations are regular rather than singular because the lowest order, Stokes flow, does not need to be corrected for inertia far away from the particle. Lift formulas arising from regular perturbations are proportional to ρ and to bilinear and quadratic powers of prescribed data $U_s, \dot{\gamma}, \Omega$ for Stokes flow; the viscosity η does not enter into the coefficients of the lift as in the singularly perturbed problems studied by Bretherton 1967 and by Saffman 1965 (X.12-X.14).

There is no need to consider singular perturbations in channels of width less than l; the region above a wall can also fall in this class, if the particle does not move so far away that the ratio

$$\left| \frac{\rho \mathbf{u} \cdot \nabla \mathbf{u}}{\eta \nabla^2 \mathbf{u}} \right| \tag{X.21}$$

is not uniformly small. This fortunate condition could apply to the uniform suspension of heavy particles against gravity.

An excellent review of literature on lift and migration of single spheres in low Reynolds number flows can be found in the paper by Cherukat and McLaughlin 1994. All of the papers except Leighton and Acrivos 1985 and Krishnan and Leighton 1995 require also that the radius of the sphere be small compared to the distance between the sphere and the wall and treat the particle as a point or forced doublet. A consequence of this additional assumption is to interdict the study of the effects of the angular velocity of the sphere on lift.

Cox and Brenner 1968 introduced the idea that inertial perturbations of Stokes flow could be carried out in regions in which the ratio (X.21) is uniformly small. Cox and Hsu 1977 computed

the lift for inertial perturbations of Stokes flow for a sedimenting sphere and for spheres in linear and quadratic flows.

The inertial lift on a sphere translating in a shear flow bounded by a single flat infinite wall was analyzed by McLaughlin 1993. He derived an expression for the lift force by superposition of the disturbance flow created by the wall and the migration velocity due to an unbounded shear field. The analysis required asymptotic matching in the far field but it converges to the regular perturbation formula (X.22) of Cox and Hsu 1977 when the distance from the wall decreases. An analytical form for the lift

$$L = 6\pi\eta a \upsilon_m \,, \tag{X.22}$$

$$\upsilon_m = \frac{-0.2855\, a U_s}{l^{*5/3}} \left(\dot{\gamma} / \nu \right)^{1/2} \tag{X.23}$$

where

$$l^* = l \left(\dot{\gamma} / \nu \right)^{1/2}$$

and υ_m is the migration velocity, is valid for large separation, $l^* >> 1$. When $\dot{\gamma}$ is negative $\dot{\gamma}$ is replaced (X.20) by $|\dot{\gamma}|$ and the minus sign is replaced by plus; the particle migrates in an opposite sense.

▪ Curvature

Gradients of shear (curvature) produce lateral forces. At the centerline of a Poiseuille flow the shear vanishes, but the shear gradient does not. To understand the Segré-Silberberg effect it is necessary to know that the curvature of the velocity profile at the center of Poiseuille flow makes the center of the channel run unstable position of equilibrium. A particle at the center of the channel or pipe will be driven by shear gradients toward the wall; a particle near the wall will lag the fluid and be driven away from the wall. An equilibrium radius away from the center and wall must exist.

Ho and Leal 1974 were the first to combine these effects in an analysis of the motion of a neutrally buoyant sphere rotating freely between plane walls so closely spaced that the inertial lift can be obtained by perturbing Stokes flow with inertia. They treated wall effects by a method of reflection and found that

$$L = 36\rho \frac{a^4}{l^2} U_m^2 (1-2\beta)\left[(1-2\beta)G_1(\beta) - G_2(\beta)\right]$$

where $\beta = x/e$ and $G_1(\beta)$, $G_2(\beta)$ are functions whose values are given in their paper; the equilibrium positions are the center line $\beta = 0.5$, which is unstable, and $\beta = 0.2$ and 0.8, which is 0.6 a from the center. This expression is valid when the sphere is not close to a wall. Vasseur and Cox 1976 used another method to treat wall effects and their results are close to Ho and Leal's near the center line but rather different than those of Ho and Leal near the wall. The requirement

$a/l << 1$ prevents them from obtaining results just next to the wall. Feng, Hu and Joseph 1994 studied the motion of solid circles in plane Poiseuille flow by DNS. The circle migrates to the 0.6 of a radius equilibrium position. They compared their 2D results with those of Ho & Leal and Vasseur & Cox.

The experiments of Segré & Silberberg 1961, 1962 do not satisfy the condition of low Reynolds number or those required to carry out an inertial perturbation of Stokes flow without asymptotic matching using Oseen's solution. Schonberg and Hinch 1989 analyzed the lift on a neutrally buoyant small sphere in a plane Poiseuille flow using matched asymptotic methods. The same problem for neutrally buoyant and non-neutrally buoyant small sphere studies using asymptotic method by Asmolov. The Reynolds numbers based on the slip velocity is small for both analyses but there is no explicit condition on the channel Reynolds number. Asmolov 1999 found that

> … wall induced inertia is significant in thin layers near the walls where the lift is closed to that calculated for linear shear flow, bounded by a single wall. In the major portion of the flow, excluding near-wall layers, the wall effect can be treated as unbounded parabolic shear flow. The effect of the curvature of the unperturbed velocity is significant, and the lift differs from the values corresponding to linear shear flow even at large Reynolds numbers.

The analyses mentioned in the paragraph above take the effect of inertia $(\mathbf{u}\bullet\nabla)\mathbf{u}$ into account only in an Oseen linear system; the comparison of the results of these analyses with experiments is far from perfect. The analysis is heavy and explicit formulae for lift are not obtained.

▪ Regular perturbation in the wall region

The question addressed here is whether the regular perturbation of Stokes flow with inertia in regions dominated by viscosity (X.20) is analytic in the Reynolds number. To be precise about this we may think that the l in (X.20) is the distance between plane walls and consider steady motion of a sphere in a plane Poiseuille flow as was considered by Cox & Brenner 1968, Ho & Leal 1974, Cox & Hsu 1977 and Vasseur & Cox 1976. In the neutrally buoyant case these authors look for solutions of the form

$$\begin{bmatrix}\mathbf{u}\\ p\end{bmatrix}=\begin{bmatrix}\mathbf{u}_0\\ p_0\end{bmatrix}+\begin{bmatrix}\mathbf{u}_1\\ p_1\end{bmatrix}R+O(R) \qquad \text{(X.24)}$$

where say $R=U_m l/\nu$ and $\mathbf{u}_0$, p_0 are Stokes flow. The Stokes flow is degenerated in that the sphere can move parallel to a wall at any distance $\beta = x/l$, but steady solutions will arise only when the sphere is at a position of equilibrium and doesn't migrate. These are the Segré & Silberberg positions of equilibrium. The little $O(R)$ is not specified in these studies because it is not needed. It seems probable to me that in the equilibrium case of an R family of steady solutions of non-migrating spheres the solution is analytic and may be represented by power series

$$\begin{bmatrix} \mathbf{u} \\ p \end{bmatrix} = \sum_{n=0}^{\infty} \begin{bmatrix} \mathbf{u}_n \\ p_n \end{bmatrix} R^n \tag{X.25}$$

Consider the perturbation problems for the steady motion $\mathbf{U} = \mathbf{e}_x U$ of a sphere parallel to the stationary walls of a Poiseuille flow $\mathbf{u} = \mathbf{e}_x \tilde{u}(y)$, as in figure IX.2. The equations are made dimensionless with *a* and *U*, *R = Ua/ν*, and they are written in a coordinate system fixed on the sphere. The equations are

$$R(\mathbf{u} \bullet \nabla)\mathbf{u} = \operatorname{div} \boldsymbol{\sigma}[\mathbf{u}], \ \operatorname{div} \mathbf{u} = 0 \tag{X.26}$$

$$\left.\begin{aligned} &\mathbf{u} = (\boldsymbol{\Omega}/U) \wedge \mathbf{x}, \quad |\mathbf{x}| = 1 \\ &\mathbf{u} = -1\mathbf{e}_x \quad \text{on the walls} \\ &\mathbf{u} = (\tilde{u}(y)/U - 1)\mathbf{e}_x \ \text{ as } |\mathbf{x}| \to \infty \end{aligned}\right\} \tag{X.27}$$

where

$$\operatorname{div} \boldsymbol{\sigma}[\mathbf{u}] = -\nabla p + \nabla^2 \mathbf{u} \, . \tag{X.28}$$

At zeroth order, Stokes flow, we have

$$\operatorname{div} \boldsymbol{\sigma}[\mathbf{u}_0] = 0, \operatorname{div} \mathbf{u}_0 \tag{X.29}$$

where $\mathbf{u}_0$ satisfies the conditions (X.27). Higher order problems are in the form *n* = 1, 2, …

$$\begin{cases} \mathbf{f}_n(\mathbf{u}_0, \mathbf{u}_1, \ldots \mathbf{u}_{n-1}) = \operatorname{div} \boldsymbol{\sigma}[\mathbf{u}_n], \operatorname{div} \mathbf{u}_n = 0 \\ \mathbf{u}_n = 0 \begin{cases} \text{on } |\mathbf{x}| = 1 \\ \text{on the wall} \\ \text{at infinity} \end{cases} \end{cases} \tag{X.30}$$

where $\mathbf{f}_n$ depends on only solutions at lower order $\mathbf{u}_m$, $m < n$. For example

$$\mathbf{f}(\mathbf{u}_0) = (\mathbf{u}_0 \bullet \nabla)\mathbf{u}_0 \ . \tag{X.31}$$

The lift-off problem for non-neutrally particles which was studied by DNS in chapter IX is not conveniently framed as a power series, since lift-off occurs at a finite Reynolds number; below this the particle slides and rolls and the sliding and rolling might be generated as a power series. Another possibility would be to develop the steady forward motion of a heavy sphere or cylinder subject to zero torque and net force, with lift balancing buoyant weight as a power series in the Reynolds number, which is zero at lift-off.

It is something of a mathematical mystery as just why it is that the solution of the problem of a sphere moving forward in an infinite domain is not analytic as can be seen already in the lift formulas (X.12) of Bretherton 1962 and (X.13) of Saffman 1965. The drag formula for a single sphere of a radius *a* moving forward with velocity *U* in an infinite fluid which was derived by Proudman and Pearson 1957

$$D = 6\pi\eta aU\left[1+\frac{3}{8}R+\frac{9}{40}R^2\ln R+O(R^2)\right]$$

where $R = au/v$ does not reverse sign automatically when the sphere velocity is reversed; conditions specified by T.B. Benjamin 1993 are required to guarantee the required symmetry.

▪ Reciprocal theorem

The lift on a sphere translating parallel to a wall may be assumed to be a power series

$$L = \sum_{n=0} L_n R^n . \tag{X.32}$$

The reciprocal theorem of Lorenz can be used to show that the lift coefficient at order n may be computed on a solutions of lower order $m < n$. The same kind of analysis can be used to compute the migration velocity perpendicular to the wall when this migration is not suppressed as shown first by Cox 1965 and comprehensively by Ho & Leal 1974. The proof of the reciprocal theorem given below applies to the problem studied by Cherakut & McLaughlin 1994 and generalized the result for L_1 to L_n.

Consider an auxiliary Stokes flow problem between flat wall

$$\left.\begin{aligned} &\operatorname{div}\boldsymbol{\sigma}[\mathbf{q}] = 0,\ \operatorname{div}\mathbf{q} = 0 \\ &\mathbf{q} = \mathbf{e}_y \ \text{ on } \ |\mathbf{x}| = 1 \\ &\mathbf{q} = 0 \ \text{ on the wall and at } \infty \end{aligned}\right\} \tag{X.33}$$

Using (X.30), we form the integral

$$\int_V \left(\mathbf{q}\bullet\operatorname{div}\boldsymbol{\sigma}[\mathbf{u}_n] - \mathbf{u}_n\bullet\operatorname{div}\boldsymbol{\sigma}[\mathbf{q}]\right)\mathrm{d}V = \int_V \mathbf{q}\bullet\mathbf{f}_n\,\mathrm{d}V$$

where V is the region occupied by fluid. Using the divergence theorem and the boundary conditions $\left(\mathbf{u}_n = 0 \text{ on } \partial V\right)$

$$\int_{\partial B} \mathbf{q}\bullet\left(\mathbf{n}\bullet\boldsymbol{\sigma}[\mathbf{u}_n]\right)\mathrm{d}A + I = \int_V \mathbf{q}\bullet\mathbf{f}_n\,\mathrm{d}V \tag{X.34}$$

where A is an element of area on the boundary ∂B of the sphere B and

$$\begin{aligned} I &= \int_V \left(-\frac{\partial q_i}{\partial x_j}\sigma_{ij}[\mathbf{u}_n] + \frac{\partial u_{ni}}{\partial x_j}\sigma_{ij}[\mathbf{q}]\right)\mathrm{d}V \\ &= \int_V \left\{-D_{ij}[q]\left(-p[\mathbf{u}_n]\delta_{ij} + D_{ij}[\mathbf{u}_n]\right) + D_{ij}[\mathbf{u}_n]\left(-p[\mathbf{q}]\delta_{ij} + D_{ij}[\mathbf{q}]\right)\right\}\mathrm{d}V \\ &= \int_V \left(p[\mathbf{u}_n]\operatorname{div}\mathbf{q} - p[\mathbf{q}]\operatorname{div}\mathbf{u}_n\right)\mathrm{d}V = 0. \end{aligned}$$

Hence, using $\mathbf{q} = \mathbf{e}_y$ on $|\mathbf{x}| = 1$, we get

$$L_n = \int_{\partial B} \mathbf{e}_y \bullet \left(\mathbf{n} \bullet \boldsymbol{\sigma}[\mathbf{u}_n]\right) \mathrm{d}A + I = \int_V \mathbf{q} \bullet \mathbf{f}_n \, \mathrm{d}V \ . \tag{X.35}$$

Since $\mathbf{f}_n$ depends on $\mathbf{U}_m$, $m < n$, so does L_n. Using (X.31), we get

$$L_1 = \int_V \mathbf{q} \bullet \left((\mathbf{u} \bullet \nabla)\mathbf{u}_0\right) \mathrm{d}V \ . \tag{X.36}$$

In the low R analysis given in the sequel we mean L_1 when we write L .

▪ Finite size sphere near a wall

Leighton & Acrivos 1985, Cherakut & McLaughlin 1994 and Krishnan & Leighton 1995 have studied the inertial lift of finite size spheres as a perturbation of Stokes flow in the near wall region.

Leighton & Acrivos 1985 evaluated the lift on a stationary sphere in a shear flow to the lowest order in the Reynolds when the sphere touches the wall; the lift points away from the wall and varies as the fourth power of the radius of the sphere and the square of the shear rate.

Cherakut & McLaughlin 1994 derived an expression for the lift of a spherical particle in a linear shear flow perturbing Stokes flow. They represented the sphere and the wall in a bi-polar spherical coordinate system (ξ, η, ϕ) and an associated cylindrical polar coordinate system. The coordinate $\xi = \alpha$ corresponds to the sphere (the center of the sphere being located at $z = l$, $\rho = 0$) and the coordinate surface $\xi = 0$ corresponds to a sphere of infinite radius which coincides with the wall. The bispherical solution method breaks down as the separation distance between the sphere and the wall vanishes; results were obtained for sphere-wall separations greater or equal to 0.1 radius.

The Stokes flow solution for steady solutions of a sphere moving parallel to a wall requires selection of the distance from the wall. Leighton & Acrivos 1985 and Krishnan & Leighton 1995 put this separation to zero, the sphere touches the wall. Cherakut & McLaughlin 1994 leave this distance arbitrary.

Krishnan & Leighton 1995 studied the inertial lift on a translating and rotating sphere in contact with a plane wall in a shear flow. The calculation requires three independent Stokes flow solutions for prescribed values of a translational velocity U; angular velocity $\boldsymbol{\Omega}$ and wall shear $\dot{\gamma}$. The Stokes flow solutions may be superposed.

$$\mathbf{u}_0 = \mathbf{u}_{01} U + \mathbf{u}_{02} \boldsymbol{\Omega} + \mathbf{u}_{03} \overset{\circ}{\gamma} .$$

The lift is presented in terms of quadratic and bilinear products of these coefficients

$$\begin{aligned} L/\rho \ &= 9.275 a^4 \overset{\circ}{\gamma}^{\,2} + 1.755 a^2 U^2 + 0.546 a^4 \boldsymbol{\Omega}^2 + 1.212 a^4 \overset{\circ}{\gamma} \boldsymbol{\Omega} \\ &\quad - 2.038 a^3 U \boldsymbol{\Omega} - 9.044 a^3 U \overset{\circ}{\gamma} . \end{aligned} \tag{X.37}$$

This formula is independent of viscosity.

They note that when this lift exceeds the buoyant weight, the sphere will rise ultimately to an equilibrium height *h* for which

$$L = (\rho_p - \rho)\frac{4}{3}\pi a^3 g \tag{X.38}$$

under the conditions that the net force accelerating particle and the net torque on the particle vanish. These three conditions for steady motion driven by shear of a particle parallel to a wall requires Stokes flow solutions not only when the particle touches the wall but when it is a distance *h* away from the wall. Given a translating and rotating sphere in Stokes flow in a shear field at a height *h* we may select $\Omega(h,\dot\gamma), U(h,\dot\gamma)$ so that the three contributions to the total for forward force and torque vanish:

$$D_0 = D_{01}U + D_{02}\Omega + D_{03}\overset{\circ}{\gamma} = 0\,. \tag{X.39}$$

And torque

$$T_0 = T_{01}U + T_{02}\Omega + T_{03}\overset{\circ}{\gamma} = 0\,. \tag{X.40}$$

Then (X.38) determines $h(\dot\gamma)$, the equilibrium height, and the equilibrium solution $U(\dot\gamma), \Omega(\dot\gamma), h(\dot\gamma)$.

To carry out the program outlined in the paragraph above, Krishnan & Leighton 1995 used an approximate "lubrication" solution of Stokes equations of Goldman, Cox & Brenner 1967 for the translation and rotation of a sphere parallel to a plane wall in a semi-infinite fluid when the gap width *h* is very small. Krishnan & Leighton 1995 say that the dependence of the inertial lift on *h* is relatively weak and use the formula (X.37) to compute the equilibrium *h* as a function of $\dot\gamma$.

The separation distance *h*, the forward slip velocity U_s of the sphere, the angular velocity Ω of the fluid and the shear rate $\dot\gamma$ are prescribed in the Stokes flow solutions used by Cherakut & McLaughlin 1994. This is more accurate than the lubrication solution of Goldman et al 1967 used by Krishnan & Leighton 1995. They computed the lift $L(\dot\gamma, h, U_s, \Omega)$ using the reciprocal theorem (X.36) and numerical quadrature. They find that

$$L = L = \rho V^2 a^2 I(\kappa, \Lambda_{\dot\gamma}, \Lambda_{\Omega,}\Lambda_s) \tag{X.41}$$

where $\kappa = a/h, \Lambda_{\dot\gamma} = \dot\gamma a/V, \Lambda_{\Omega,} = \Omega a/V$ and $\Lambda_s = U_s/V$. They consider the case of no rotation $\Omega = 0$ and of a freely rotating sphere taking the values of Ω computed by Goldman, Cox and Brenner 1967 for zero torque. This reduces their considerations to two families of *I* depending on $\kappa, \Lambda_{\dot\gamma}, \Lambda_s$. They studied the lift force for different prescribed values of U_s; when $U_s \neq 0,\ V = U_s,\ \Lambda_s = 1$ and $I = I(\kappa, \Lambda\dot\gamma)$ where $\Lambda_{\dot\gamma} = \dot\gamma a/U_s$. The case $U_s = 0$ corresponds to neutrally buoyant spheres in a linear shear flow when wall effects are not important; there is no slip. In this case $V = \dot\gamma a,\ \Lambda_{\dot\gamma} = 1,\ \Lambda_s = 0$.

The analysis of Cherakut & McLaughlin 1994 does not determine the slip velocity U_s. They do extensive numerical studies computing L for different choices of $\Lambda\dot{\gamma}$ and κ when $\Omega = 0$ and when the particle is freely rotating. The computed values are assembled into tables. Since $\mathbf{U}_o$ is at most a linear function of $\Lambda\dot{\gamma}$, the reciprocal theorem (X.36) shows that I is at most a quadratic polynomial in $\Lambda\dot{\gamma}$. The coefficients were expressed in powers of κ by nonlinear regression from the tables. They find that when Ω is determined from the analysis of a freely rotating sphere by Goldman, *et al* 1967

$$\begin{aligned} I = &\left[1.7631 + 0.3561\kappa - 1.1837\kappa^2 + 0.845163\kappa^3\right] \\ &-\left[\frac{3.24139}{\kappa} + 2.6760 + 0.8248\kappa - 0.4616\kappa^2\right]\Lambda_{\dot{\gamma}} \\ &+\left[1.8081 + 0.879585\kappa - 1.9009\kappa^2 + 0.98149\kappa^3\right]\Lambda_{\dot{\gamma}}^2 . \end{aligned} \tag{X.42}$$

Whereas when $\Omega = 0$, they get

$$\begin{aligned} I = &\left[1.7716 + 0.2160\kappa - 0.7292\kappa^2 + 0.4854\kappa^3\right] \\ &-\left[\frac{3.2397}{\kappa} + 1.1450 + 2.0840\kappa - 0.9059\kappa^2\right]\Lambda_{\dot{\gamma}} \\ &+\left[2.0069 + 1.0575\kappa - 2.4007\kappa^2 + 1.317\kappa^3\right]\Lambda_{\dot{\gamma}}^2 . \end{aligned} \tag{X.43}$$

Recall that $L = \rho V^2 a^2 I$, $V = U$, or $\dot{\gamma}a$ when $U_s = 0$.

The analysis of Cherakut & McLaughlin 1994 appear to agree with results obtained by Leighton & Acrivos 1985 and by Krishnan & Leighton 1995 when $\kappa = a/h$ is large and with Cox & Hsu 1977 when κ is small.

Lovalenti 1994 derived an expression for the lift force for small by modifying the results derived by Cox & Brenner 1968 and Cox & Hsu 1977 in an interesting appendix to the paper by Cherakut & McLaughlin. He finds that

$$\begin{aligned} L/\rho \;&= \frac{6\pi(61)}{4\times144}a^4\dot{\gamma}^2 + \frac{18\pi}{32}a^2U_s^2 \\ &\quad + \left\{-\frac{66}{64}\pi a^3\left(\frac{1}{\kappa}+\frac{27}{16}\right)+\frac{11}{8}\pi a^3\right\}\dot{\gamma}U_s \\ &\quad - \frac{6\pi(61)}{4\times144}\cdot\frac{12}{61}a^4\Omega\dot{\gamma} - \pi a^4\Omega U_s \\ &= 1.99622a^4\dot{\gamma}^2 + 1.76715a^4U_s^2 \\ &\quad + \left(-\frac{3.23977}{\kappa} - 1.14742\right)a^3\dot{\gamma}U_s \\ &\quad - 0.39270a^4\Omega\dot{\gamma} - 3.1415a^3\Omega U_s . \end{aligned} \tag{X.44}$$

This formula can be compared with (X.37); the term proportional to Ω^2 is absent and the signs and magnitude of the coefficients of other terms do not agree.

The expression (X.42) satisfies the condition for a freely rotating sphere. With $\dot{\gamma}$ prescribed, the lift formula (X.43) leave $h(\dot{\gamma})$ and the slip velocity $U_s(\dot{\gamma})$ undetermined. To determine these quantities we could apply the lift-buoyant weight balance, as in (X.25) and a zero force balance.

REMOVE THIS PAGE (only used to generate table of contents)